BNL - 65801

Synchrotron Radiation Sources

S. L. Hulbert and G. P. Williams
Brookhaven National Laboratory
Upton, New York, USA

July 1998

National Synchrotron Light Source

Brookhaven National Laboratory
Operated by
Brookhaven Science Associates
Upton, NY 11973

Under Contract with the United States Department of Energy
Contract Number DE-AC02-98CH10886

DISCLAIMER

Methods of Vacuum Ultraviolet Spectroscopy
edited by
J.A.R. Samson and D.L. Ederer

Chapter 1. Synchrotron Radiation Sources.
by S. L. Hulbert and G.P. Williams

General Description of Synchrotron Radiation

Synchrotron radiation is a very bright, broadband, polarized, pulsed source of light extending from the infrared to the x-ray region. It is an extremely important source of Vacuum Ultraviolet radiation. Brightness is defined as flux per unit area per unit solid angle and is normally a more important quantity than flux alone particularly in throughput limited applications which include those in which monochromators are used.

It is well known from classical theory of electricity and magnetism that accelerating charges emit electromagnetic radiation. In the case of synchrotron radiation, relativistic electrons are accelerated in a circular orbit and emit electromagnetic radiation in a broad spectral range. The visible portion of this spectrum was first observed on April 24, 1947 at General Electric's Schenectady facility by Floyd Haber, a machinist working with the synchrotron team, although the first theoretical predictions were by Liénard[1] in the latter part of the 1800's. An excellent early history with references was presented by Blewett[2] and a history covering the development of the utilization of synchrotron radiation was presented by Hartman[3].

Synchrotron radiation covers the entire electromagnetic spectrum from the infrared region through the visible, ultraviolet, and into the x-ray region up to energies of many 10's of kilovolts. If the charged particles are of low mass, such as electrons, and if they are traveling relativistically, the emitted radiation is very intense and highly collimated, with opening angles of the order of 1 milliradian. In electron storage rings there are three possible sources of synchrotron radiation; dipole (bending) magnets; wigglers, which act like a sequence of bending magnets with alternating polarities; and undulators, which are also multi-period alternating magnet systems but in which the beam deflections are small resulting in coherent interference of the emitted light.

In typical storage rings used as synchrotron radiation sources, several bunches of up to ~ 10^{12} electrons circulate in vacuum, guided by magnetic fields. The bunches are typically several 10's of centimeters long, so that the light is pulsed, being on for a few 10's to a few 100's of picoseconds, and off for several 10's to a few 100's of nanoseconds depending on the particular machine and the radio-frequency cavity which restores the energy lost to synchrotron radiation. However for a ring of circumference 30m, the revolution time is 100

nanoseconds, so that each bunch of 10^{12} electrons is seen 10^7 times per second, giving a current of ~1 Ampere.
The most important characteristic of accelerators built specifically as synchrotron radiation sources is that they have a magnetic focusing system which is designed to concentrate the electrons into bunches of very small cross-section and to keep the electron transverse velocities small. The combination of high intensity with small opening angles and small source dimensions results in the very high brightness.
The first synchrotron radiation sources to be used were operated parasitically on existing high energy physics or accelerator development programs. These were not optimized for brightness, and were usually accelerators rather than storage rings, meaning that the electron beams were constantly being injected, accelerated and extracted. Owing to the successful use of these sources for scientific programs, a second generation of dedicated storage rings was built starting in the early 1980's. In the mid 1990's, a third generation of sources was built, this time based largely on special magnetic insertions called undulators and wigglers. A fourth generation is also under development based on what is called multiparticle coherent emission, in which coherence along the path of the electrons, or longitudinal coherence, plays the major role. This is achieved by microbunching the electrons on a length scale comparable to or smaller than the scale of the wavelengths emitted. The emission is then proportional to the square of the number of electrons, N, which, if N is 10^{12}, can be a very large enhancement. These sources can reach the theoretical diffraction limit of source emittance (the product of solid angle and area).

Theory of Synchrotron Radiation Emission.

General

The theory describing synchrotron radiation emission is based on classical electrodynamics and can be found in the works of Tomboulian and Hartman[4] (1956), Schwinger[5] (1949), Jackson[6] (1975), Winick[7] (1980), Hofmann[8] (1980), Krinsky, Perlman and Watson[9] (1983) and Kim[10] (1989). A quantum description, presented by Sokolov and Ternov[11](1968), is quantitavely equivalent.
Here we present a phenomenological description in order to highlight the general concepts involved. Electrons in circular motion radiate in a dipole pattern as shown schematically in Fig. 1a. As the electron energies increase and the particles start traveling at relativistic velocities, this dipole pattern appears different to an observer in the rest frame of the laboratory. To find out how this relativistic dipole pattern appears to the observer at rest, we need only appeal to standard relativity theory. This tells us that angles θ_t in a transmitting object are related to those in the receiving frame, θ_r, by:

$$\tan\theta_r = \frac{\sin\theta_t}{\gamma\ (\cos\theta_t - \beta\ )} \qquad (1)$$

with γ, the ratio of the mass of the electron to its rest mass, being given by E/m_oc^2, E being the electron energy, m_o the electron rest mass and c the velocity of light. β is the ratio of electron velocity, v, to the velocity of light, c. Thus for electrons at relativistic energies, $\beta \approx 1$ so the peak of the dipole emission pattern in the particle frame, θ_t=90°, transforms to $\theta_r \approx \tan \theta_r \approx \gamma^{-1}$ in the laboratory frame as shown in Fig. 1b. Thus γ^{-1} is a typical opening angle of the radiation in the laboratory frame. Now for an electron viewed in passing by an observer, as shown in Fig. 2, the duration of the pulse produced by a particle under circular motion of radius ρ will be $\rho/\gamma c$ in the particle frame, or $\rho/\gamma c$ x $1/\gamma^2$ in the laboratory frame owing to the time dilation. The Fourier transform of this function will contain frequency components up to the reciprocal of this time interval. For a storage ring with a radius of 2 meters and γ = 1000, corresponding to a stored electron beam energy of ~ 500 MeV, the time interval is 10^{17} seconds, which corresponds to light of wavelength 30 Å.

Bending Magnet Radiation.

It is useful to define a few quantities in practical units as these will be used in the calculations that follow. For an electron storage ring, the relationship between the electron beam energy E in GeV, bending radius ρ in meters and field B in T is :

$$\rho\ [m] = \frac{E[GeV]}{0.300B[T]} \qquad (2)$$

γ, the ratio of the mass of the electron to its rest mass is given by:

$$\gamma = E/m_oc^2 = E/0.511MeV = 1957\ E[GeV] \qquad (3)$$

and λ_c , which is defined as the wavelength for which half the power is emitted above and half below, is:

$$\lambda_c = 4\pi\rho/(3\gamma^3) \text{ or } \lambda_c[Å] = 5.59\ \rho[m] / E^3[GeV^3] = 18.6 / B[T]\ E^2[GeV^2] \quad (4)$$

The critical frequency and photon energy are

$$\omega_c = 2\pi c/\lambda_c = 3c\gamma^3 / (2\rho) \text{ or } \varepsilon_c(eV) = \hbar\omega_c(eV) = 665.5\ E^2[GeV^2]\ B[T] \quad (5)$$

The angular distribution of synchrotron radiation emitted by electrons moving through a bending magnet with a circular trajectory in the horizontal plane is given[9] by:

$$\frac{d^2F_{bm}(\omega)}{d\theta d\psi} = \frac{3\alpha}{4\pi^2}\gamma^2\frac{\Delta\omega}{\omega}\frac{I}{e}\left(\frac{\omega}{\omega_c}\right)^2(1+\gamma^2\psi^2)^2\left[K_{2/3}^2(\xi)+\frac{\gamma^2\psi^2}{1+\gamma^2\psi^2}K_{1/3}^2(\xi)\right] \quad (6)$$

where F is the number of photons per second, θ the observation angle in the horizontal plane, ψ the observation angle in the vertical plane, α the fine structure constant (1/137), ω is the light frequency, I the beam current, and $\xi = (\omega/2\omega_c)(1+\gamma^2\psi^2)^{3/2}$. The subscripted K's are modified Bessel functions of the second kind. The $K_{2/3}$ term represents light linearly polarized parallel to the electron orbit plane, while the $K_{1/3}$ term represents light linearly polarized perpendicular to the orbit plane.
If one integrates over all vertical angles, then the total intensity is:

$$\frac{dF_{bm}(\omega)}{d\theta} = \frac{\sqrt{3}}{2\pi}\alpha\gamma\frac{\Delta\omega}{\omega}\frac{I}{e}\frac{\omega}{\omega_c}\int_{\omega/\omega_c}^{\infty}K_{5/3}(y)dy \quad (7)$$

In practical units these formulae become:

$$\frac{d^2F_{bm}(\omega)}{d\theta\, d\psi} = 1.326\times10^{13}E^2[GeV]I[A](1+\gamma^2\psi^2)^2\left(\frac{\omega}{\omega_c}\right)^2\left[K_{2/3}^2(\xi)+\frac{\gamma^2\psi^2}{1+\gamma^2\psi^2}K_{1/3}^2(\xi)\right] \quad (8)$$

in units of photons/sec/mrad^2/0.1%bandwidth, and:

$$\frac{dF_{bm}(\omega)}{d\theta} = 2.457\times10^{13}E[GeV]I[A]\frac{\omega}{\omega_c}\int_{\omega/\omega_c}^{\infty}K_{5/3}(y)dy \quad (9)$$

photons per second per milliradian per 0.1% bandwidth.

The Bessel functions can be computed easily using algorithms of Kostroun[12]:

$$K_\nu(x) = h\left\{\frac{e^{-x}}{2}+\sum_{r=1}^{\infty}e^{-x\cosh(rh)}\cosh(\nu\, rh)\right\} \quad (10)$$

and

$$\int_x^{\infty}K_\nu(\eta)d\eta = h\left\{\frac{e^{-x}}{2}+\sum_{r=1}^{\infty}e^{-x\cosh(rh)}\frac{\cosh(\nu\, rh)}{\cosh(rh)}\right\} \quad (11)$$

for all x and for any fractional order ν, where h is some suitable interval such as 0.5. In evaluating the series, the sum is terminated when the rth. term is small, $<10^{-5}$ for example.

In Fig. 3 we plot the universal function $G_1\left(\frac{\omega}{\omega_c}\right) = \frac{\omega}{\omega_c}\int_{\frac{\omega}{\omega_c}}^{\infty}K_{5/3}(y)dy$ from Eqs. 7 or 9, so that the photon energy dependence of the flux from a given ring can be

calculated readily. It is found that the emission falls off exponentially as $e^{-\lambda_c/\lambda}$ for wavelengths shorter than λ_c, but only as $\lambda^{-1/3}$ at longer wavelengths.

The vertical angular distribution is more complicated. For a given ring and wavelength, there is a characteristic natural opening angle for the emitted light. The opening angle increases with increasing wavelength. If we define ψ as the vertical angle relative to the orbital plane, and if the vertical angular distribution of the emitted flux is assumed to be Gaussian in shape, then the rms divergence σ_ψ is calculated by taking the ratio of Eqs. 7/6 evaluated at ψ =0:

$$\sigma_\psi = \sqrt{\frac{2\pi}{3}}\frac{1}{\gamma}\left(\frac{\omega}{\omega_c}\right)^{-1}\frac{\int_{\omega/\omega_c}^{\infty} K_{5/3}(y)dy}{K_{2/3}^2(\omega/2\omega_c)} \qquad (12)$$

In reality, the distribution is not Gaussian, especially in view of the fact that the distribution for the vertically polarized component vanishes in the horizontal plane (ψ =0). However, σ_ψ defined by Eq. 12 is still a simple and useful measure of the angular divergence. Eq. 12 is of the form:

$$\sigma_\psi = \frac{1}{\gamma}C(\omega/\omega_c) \qquad (13)$$

and the function $C(\omega/\omega_c)$[10] is plotted in Fig. 4. At $\omega=\omega_c$, $\sigma_\psi \approx 0.64/\gamma$. The asymptotic values of σ_ψ can be obtained from the asymptotic values of the Bessel functions and are:

$$\sigma_\psi \approx \frac{1.07}{\gamma}\left(\frac{\omega}{\omega_c}\right)^{-1/3} ;\omega << \omega_c \qquad (14)$$

and

$$\sigma_\psi \approx \frac{0.58}{\gamma}\left(\frac{\omega}{\omega_c}\right)^{-1/2} ;\omega >> \omega_c \qquad (15)$$

In Fig. 5 we show examples of the normalized vertical angular distributions of both parallel and perpendicularly polarized synchrotron radiation for a selection of wavelengths.

Circular Polarization and Aperturing for Magnetic Circular Dichroism

Circularly polarized radiation is a valuable tool for the study of electronic, magnetic, and geometric structure of a wide variety of materials. The dichroic response in the soft x-ray spectral region (100-1500eV) is especially important because in this energy range almost every element has a strong dipole transition from a sharp core level to its lowest unoccupied state[13].

The production of bright sources of circularly polarized *soft x-rays* is therefore a topic of keen interest, and is a problem which has seen a multitude of solutions, from special insertion devices (crossed undulators, helical undulators, elliptically polarized undulators/wigglers) to optical devices (multiple-bounce reflectors/multilayers and quarter-wave plates). However, standard bending magnet synchrotron radiation sources are good sources of elliptically polarized soft x-rays when viewed from either above or below the orbital plane.

As discussed by Chen[13], a practical solution involves acceptance of a finite vertical angular range, $\psi_{off} - \Delta\psi/2 < \psi < \psi_{off} + \Delta\psi/2$ centered about any vertical offset angle $\psi = \psi_{off}$ or, equivalently, about $\psi = -\psi_{off}$. This slice of bending magnet radiation exhibits a circular polarization[14]

$$P_c = -\frac{2A_h A_v}{(A_h^2 + A_v^2)} \qquad (16)$$

where $A_h = K_{2/3}(\xi)$ and $A_v = \gamma\psi/(1+\gamma^2\psi^2)^{1/2}K_{1/3}(\xi)$ are proportional to the square-roots of the horizontally and vertically polarized components of bending magnet flux (Eq. 8), i.e A_h and A_v are proportional to the horizontal and vertical components of the electric field, respectively. P_c depends on the vertical angle ψ, electron energy γ and, through ξ, the emitted photon energy ω/ω_c. In Fig. 6 we plot values of P_c vs $\gamma\psi$ and ω/ω_c for γ=1565 (E=0.8GeV) and ρ=1.91m ($h\nu_{crit}$=594 eV).

Magnetic circular dichroism (MCD) measures the normalized difference of the absorption of right circular and left circular light. Assuming no systematic error, the signal to noise ratio in such a measurement defines a figure of merit

$$MCD\ figure\ of\ merit = (average\ circular\ polarization) \times (flux\ fraction)^{1/2} \qquad (17)$$

where

$$average\ circular\ polarization = \frac{\int_{\psi_{off}-\frac{\Delta\psi}{2}}^{\psi_{off}+\frac{\Delta\psi}{2}} P_c(\psi)\frac{dF}{d\psi}d\psi}{\int_{\psi_{off}-\frac{\Delta\psi}{2}}^{\psi_{off}+\frac{\Delta\psi}{2}} \frac{dF}{d\psi}d\psi} \qquad (18)$$

and the fraction of the total (vertically-integrated) flux emitted into the vertical slice $\psi = \psi_{off} \pm \Delta\psi/2$ is:

$$flux\ fraction = \frac{1}{dF_{bm}(\omega)/d\theta} \int_{\psi_{off}-\Delta\psi/2}^{\psi_{off}+\Delta\psi/2} \frac{d^2F_{bm}(\omega)}{d\theta d\psi} d\psi \qquad (19)$$

Here $d^2F_{bm}(\omega)/d\theta d\psi$ is the angular dependence of the bending magnetic flux from Eq. 8 and $dF_{bm}(\omega)/d\theta$ is the vertically integrated flux from Eq. 9. For an 0.8 GeV storage ring (e.g. NSLS VUV), the best choices of ψ and $\Delta\psi$ are 0.5 mrad and 0.66 mrad respectively. This yields a flux fraction ~ 0.3, a circular polarization ~ 0.65 and a figure of merit ~ 0.35.

Bending Magnet Power

Integration of $I/e\hbar\omega d^2F_{bm}(\omega)/d\theta d\psi$ from Eq. 8 over all frequencies ω yields the angular distribution of power radiated by a bending magnet:

$$\frac{d^2P_{bm}}{d\theta d\psi} = \frac{I}{e}\int_0^\infty \hbar\omega \frac{d^2F_{bm}(\omega)}{d\theta d\psi} d\omega = \frac{I}{e}\frac{\alpha hc\gamma^5}{2\pi\rho}\frac{7}{16}F(\gamma\psi) \qquad (20)$$

which is independent of the horizontal angle θ as required by symmetry, and the vertical angular dependence is contained in the factor

$$F(\gamma\psi\ ) = \frac{1}{(1+\gamma\psi^2)^{5/2}}\left[1+\frac{5}{7}\frac{\gamma^2\psi^2}{(1+\gamma^2\psi^2)}\right]. \qquad (21)$$

The first term in $F(\gamma\psi)$ represents the component of the bending magnet radiation parallel to the orbital plane, while the second represents the perpendicular polarization component. $F(\gamma\psi)$ and its polarization components are plotted vs $\gamma\psi$ in Fig. 7. Note that the area under the $F_{parallel}$ curve is approximately seven times greater than that for $F_{perpendicular}$.

In practical units,

$$\frac{d^2P_{bm}}{d\theta d\psi}(W/mrad^2) = \frac{18.082E^5[GeV^5]I[A]}{\rho\ [m]}F(\gamma\psi) \qquad (22)$$

Integrating Eq. 20 over the out-of-orbital-plane (vertical) angle ψ yields the total power radiated per unit in-orbital-plane (horizontal) angle θ:

$$\frac{dP_{bm}}{d\theta} = \frac{1}{3\pi}\frac{I}{e}\frac{hc\alpha\gamma^4}{\rho} \qquad (23)$$

or, in practical units,

$$\frac{dP_{bm}}{d\theta}(W/mrad) = \frac{14.080E^4[GeV^4]I[A]}{\rho\ [m]} \qquad (24)$$

For example, a 1.0 GeV storage ring with 2 m radius bends generates 7.04 W/mrad per Amp of stored current. By contrast, a 2.5 GeV machine with 7 m radius bends generates 78.6 W/mrad/A and a 7 GeV machine with 39 m radius bends generates 867 W/mrad/A.

Bending Magnet Brightness.

Thus far we have calculated the emitted flux in photons per second per milliradian^2 of solid angle. In order to calculate the brightness we need to include the source size. In these calculations we calculate the central (or maximum) brightness, for which we use the natural opening angle to define both the horizontal and vertical angles. Using vertical angles larger than this will not increase the flux as there is no emission. Using larger horizontal angles will increase the flux proportionately as all horizontal angles are filled with light, but owing to the curvature of the electron trajectory, the *average* brightness will actually be less. The brightness expression[17,18] is:

$$B_{bm} = \frac{\left.\frac{d^2F_{bm}}{(d\theta\ d\psi)}\right|_{\psi=0}}{2\pi\sum_x\sum_y} \qquad (25)$$

where:

$$\sum_x = [\varepsilon_x\beta_x + \eta_x^2\sigma_E^2 + \sigma_r^2]^{1/2} \qquad (26)$$

and

$$\sum_y = \left[\varepsilon_y\beta_y + \sigma_r^2 + \frac{\varepsilon_y^2 + \varepsilon_y\gamma_y\sigma_r^2}{\sigma_\psi^2}\right] \qquad (27)$$

where ε_x and ε_y are the electron beam emittances in the horizontal and vertical directions respectively, β_x and β_y are the electron beam beta functions in the horizontal and vertical planes, η_x is the dispersion function in the horizontal plane and σ_E is the rms value of the relative energy spread. All the electron beam parameters are properties of a particular storage ring. The diffraction limited source size is $\sigma_r=\lambda/4\pi\sigma_\psi$. The effective source sizes ($\sum_x$ and $\sum_y$) are photon energy dependent via the natural opening angle σ_ψ and the diffraction limited source size σ_r.

Insertion Devices (Undulators and Wigglers)

General

Insertion devices are periodic magnetic structures installed in straight sections of storage rings, as illustrated in Fig. 8, in which the vertical magnetic field varies approximately sinusoidally along the axis of the undulator. The resulting motion of the electrons is also approximately sinusoidal, but in the horizontal plane. We can understand the nature of the spectra emitted from these devices by again studying the electric field as a function of time, and this is shown in Fig. 9. This shows that the electric field and hence its Fourier transform, the spectrum, depend critically on the magnitude of the beam deflection in the device. At one extreme, when the magnetic fields are high, as in Fig. 9a, the deflection is large and the electric field is a series of pulses similar to those obtained from a dipole. Such a device is termed a "wiggler". The Fourier transform for the wiggler is N times that from a single dipole. At the other extreme, as in Fig. 9b, the deflection of the electron beam is such that the electric field as a function of time is sinusoidal, and the Fourier transform is then a single peak with a width proportional to the inverse of the length of the wavetrain, L^*, according to $\lambda^2/\Delta\lambda=L^*$. L^* is obtained by dividing the real length of the device, L, by γ^2 because of relativistic effects. Thus for a meter long device emitting at a wavelength λ = 10 nm in a machine of energy 0.5 GeV ($\gamma \sim 1000$), we get $\lambda^2/\Delta\lambda = 10^{-6}$ meters, and $\lambda/\Delta\lambda = 1000$. Interference occurs in an undulator since the electric field from one part of the electron path is added coherently to that from adjacent parts.

Formal Treatment

We assume that the motion of an electron in an insertion device is sinusoidal, and that we have a field in the vertical (y) direction varying periodically along the z direction, with:

$$B_y = -B_o \sin(2\pi\, z/\lambda_u), \qquad 0 \le z \le N\lambda_u \qquad (28)$$

where B_0 is the peak magnetic field, λ_u is the period length, and N the number of periods. By integrating the equation of motion, the electron transverse velocity $c\beta_x$ is found to be:

$$\beta_x = \frac{K}{\gamma}\cos(2\pi\, z/\lambda_u) \qquad (29)$$

where

$$K = eB_o\lambda_u/2\pi mc = 0.934\lambda_u[cm]B_o[T] \qquad (30)$$

is a dimensionless parameter which is proportional to the deflection of the electron beam. The maximum slope of the electron trajectory is:

$$\delta = \frac{K}{\gamma} \qquad (31)$$

In terms of δ, we define an undulator as a device in which $\delta \le \gamma^{-1}$, which corresponds to $K \le 1$. When K is large, the device is called a wiggler. In most

insertion devices the field can be changed either electromagnetically or mechanically, and in some cases K can vary between the two extremes of undulator and wiggler operation.

Wigglers

For the wiggler, the flux distribution is given by 2N (where N is the number of magnetic periods) times the appropriate bending magnet formulae in Eqs. 8 and 9. However, ρ or B must be taken at the point in the path of the electron which is tangent to the direction of observation. For a horizontal angle θ,

$$\varepsilon_c(\theta) = \varepsilon_{c\max}\sqrt{1-(\theta/\delta)^2} \qquad (32)$$

where

$$\varepsilon_{c\max}[KeV] = 0.665E^2[GeV]B_o[T] \qquad (33)$$

Integration over θ, which is usually performed numerically, gives the wiggler flux.

The calculation of the brightness of wigglers needs to take into account the depth-of-field effects, i.e the contribution to the apparent source size from different poles. The expression for the brightness of wigglers is:

$$B_W = \frac{d^2F_W}{d\theta\, d\psi}\sum_{\pm}\sum_{n=-\frac{1}{2}N}^{\frac{1}{2}N}\frac{1}{2\pi}\times\frac{\exp\left[-\frac{1}{2}\left(\frac{x_o^2}{\sigma_x^2+z_{n\pm}^2\sigma_x'^2}\right)\right]}{\left[\left(\sigma_x^2+z_{n\pm}^2\sigma_x'^2\right)\left(\frac{\varepsilon_y^2}{\sigma_\psi^2}+\sigma_y^2+z_{n\pm}^2\sigma_y'^2\right)\right]} \qquad (34)$$

where $z_{n\pm}=\lambda_w\left(n\pm\frac{1}{4}\right)$, λ_w is the wiggler period, and σ_ψ is identical to Eq. 11, but evaluated, in the wiggler case, as the instantaneous radius at the tangent to the straight-ahead (θ=ψ=0) direction (i.e. minimum ρ, maximum ε_c), $\sigma_x=\sqrt{\varepsilon_x\beta_x}$ and $\sigma_y=\sqrt{\varepsilon_y\beta_y}$ are the rms transverse beam sizes, while $\sigma_x'=\sqrt{\varepsilon_x/\beta_x}$ and $\sigma_y'=\sqrt{\varepsilon_y/\beta_y}$ are the angular divergences of the electron beam in the horizontal and vertical directions respectively. The exponential factor in Eq. 34 arises because wigglers have two source points separated by $2x_o$, where:

$$x_0=\frac{K}{\gamma}\frac{\lambda_w}{2\pi} \qquad (35).$$

The summations in Eq. 34 must be performed for each photon energy because σ_ψ is photon energy dependent.

Undulators.

The interference which occurs in an undulator, i.e. when K is moderate ($K \leq 1$) produces sharp peaks in the forward direction at a fundamental (n=1) and all odd harmonics (n=3,5,7...) as shown for a zero emittance (ε=0) electron beam in Fig. 10(a) (dotted line). In the ε=0 case, the even harmonics (n=2,4,6,...) peak off-axis and do not appear in the forward direction. For real ($\varepsilon \neq 0$) electron beams, the spectral shape, angular distribution, and peak brightness are strongly dependent on the emittance and energy spread of the electron beam as well as the period and magnitude of the insertion device field.

In general, the effect of electron beam emittance is to cause all harmonics to appear in the forward direction (solid line in Fig. 10(a)). The effect of angle integration on the spectrum in Fig. 10(a) is shown in Fig. 10(b), a spectrum which is independent of electron beam emittance except for the presence of "noise" in the zero emittance case. The effect of electron beam emittance on the angular distribution of the fundamental, second, and third harmonics of this device is shown in Fig. 10(c), which also nicely demonstrates the dependence on harmonic number.

The peak wavelengths of the emitted radiation, λ_n, are given by:

$$\lambda_n = \frac{\lambda_u}{2n\gamma^2}\left(1+\frac{K^2}{2}+\gamma^2\theta^2\right) \qquad (36)$$

where λ_u is the undulator period length. They soften as the square of the deviation angle θ away from the forward direction.

Of main interest is the intense central cone of radiation. An approximate formula for flux integrated over the central cone is (for the odd harmonics):

$$F_u(K,\omega) = \pi\alpha N \frac{\Delta\omega}{\omega}\frac{I}{e}Q_n(K),\ n=1,3,5 \qquad (37)$$

where

$$Q_n(K) = \left(1+\frac{K^2}{2}\right)\frac{F_n(K)}{n},\ n=1,3,5 \qquad (38)$$

and

$$F_n(K) = \frac{K^2 n^2}{(1+K^2/2)^2}\left\{J_{(n-1)/2}\left[\frac{nK^2}{4\left(1+\frac{1}{2}K^2\right)}\right] - J_{(n+1)/2}\left[\frac{nK^2}{4\left(1+\frac{1}{2}K^2\right)}\right]\right\}^2 \qquad (39)$$

In practical units the flux in photons/s/0.1%bandwidth is given by:

$$F_u(K) = 1.431\times 10^{14} N Q_n(K) I[A] \qquad (40)$$

To calculate the undulator flux angular distribution and spectral output into arbitrary solid angle, one can use freely available codes such as Urgent[17] (R. P. Walker and B. Diviacco). To include magnetic field errors (e.g. measured values), use Ur[18] (R. J. Dejus and A. Luccio).

The brightness of an undulator, B_u, is approximated by dividing the central cone flux by the effective angular divergence, $\Sigma'_x(\Sigma'_y)$, and by the effective source size, $\Sigma_x(\Sigma_y)$, in the horizontal (vertical) directions. These are given by convolution of the Gaussian distributions of the electron beam and the diffraction limited photon beam, in both space and angle:

$$\Sigma_{x'} = \sqrt{{\sigma_{x'}}^2 + {\sigma_{r'}}^2}, \quad \Sigma_{y'} = \sqrt{{\sigma_{y'}}^2 + {\sigma_{r'}}^2} \tag{41}$$

$$\Sigma_x = \sqrt{\sigma_x^2 + {\sigma_r}^2}, \quad \Sigma_y = \sqrt{\sigma_y^2 + \sigma_r^2} \tag{42}$$

Thus, B_u is given by:

$$B_u = \frac{F_u}{(2\pi)^2 \Sigma_x \Sigma_y \Sigma'_x \Sigma'_y} \tag{43}$$

The diffraction limited emittance of a photon beam is the minimum value in the inequality

$$\varepsilon_r = \sigma\sigma_{r'} \geq \frac{\lambda\!\!\!^{-}}{2} = \frac{\lambda}{4\pi} \tag{44}$$

where ε is the photon emittance and λ is the wavelength, in direct analogy to the Heisenberg uncertainty principle in non-relativistic quantum mechanics. The space versus angle separation of this minimum emittance is energy and harmonic dependent[19]. For the exact harmonic frequency in the forward direction, given by Eq. 36 with θ=0, there appears to be consensus that σ_r and $\sigma_{r'}$ are given by:

$$\sigma_{r'} = \sqrt{\frac{\lambda}{2L}}, \quad \sigma_r = \frac{\sqrt{2\lambda L}}{4\pi} \tag{45}$$

On the other hand, at the peak of the angle-integrated undulator spectrum, which lies a factor of $\left(1 - \frac{1}{nN}\right)$ below the exact harmonic energy, σ_r and $\sigma_{r'}$ are given by:

$$\sigma_{r'} = \sqrt{\frac{\lambda}{L}}, \quad \sigma_r = \frac{\sqrt{\lambda L}}{4\pi} \tag{46}$$

It is clear from Eqs. 41 and 42 that the choice of expression for σ_r and $\sigma_{r'}$ can have a non-negligible effect on the undulator brightness value especially for small beam size and opening angle. Lacking a functional form for σ_r and $\sigma_{r'}$ as a function of photon energy, we shall use Eq. 46 in evaluating the expression for undulator peak spectral brightness from Eq. 43.

In Figs 11 and 12 we show calculations based on the above equations for the output flux and brightness for three synchrotron radiation facilities, the NSLS, Brookhaven National Laboratory, Upton, NY, the Advanced Light Source, Lawrence Berkeley National Laboratory, Berkeley, CA, and the Advanced Photon Source, Argonne National Laboratory, Argonne, IL, all in the USA. These sources are representative of most of the facilities around the world, their characteristics being summarized in Table 1. For undulators the brightness in the first harmonic is plotted.

Insertion device power

The Schwinger[5] formula for the distribution of radiated power from an electron in a sinusoidal trajectory, which applies with reasonable approximation to undulators and, to a lesser extent, wigglers, reduces[20] to:

$$\frac{d^2P}{d\theta d\psi} = P_{total}\frac{21\gamma^2}{16\pi K}G(K)f_K(\gamma\theta,\gamma\psi) \qquad (47)$$

where the total (angle-integrated) radiated power is

$$P_{total} = \frac{N}{6}\frac{Z_0 I 2\pi ec}{\lambda_u}\gamma^2 K^2 \qquad (48)$$

or, in practical units,

$$P_{total}[W] = 633.0E^2[GeV^2]B_0^2[T^2]L[m]I[A] \qquad (49)$$

where N is the number of undulator or wiggler periods, Z_0 is the vacuum impedance (377Ω), I is the storage ring current, e is the electronic charge, c is the speed of light, $L = N\lambda_u$ is the length of the insertion device,

$$G(K) = \frac{K}{(1+K^2)^{7/2}}\left(K^6 + \frac{24}{7}K^4 + 4K^2 + \frac{16}{7}\right) \qquad (50)$$

and

$$f_k(\gamma\theta,\gamma\psi) = \frac{16K}{7\pi\ G(K)}\int_{-\pi}^{\pi} d\alpha\left(\frac{1}{D^3} - \frac{4(\gamma\theta - K\cos\alpha)^2}{D^5}\right)\sin^2\alpha \qquad (51)$$

where

$$D = 1 + \gamma^2\psi^2 + (\gamma\theta - K\cos\alpha)^2 . \qquad (52)$$

The integral in the expression for f_K is best evaluated numerically.

For K>1, which includes all wigglers and much of the useful range of undulators, an approximate formula for the angle dependence of the radiated power is

$$f_K(\gamma\theta,\gamma\psi) = \sqrt{1-\left(\frac{\gamma\theta}{K}\right)^2}\; F(\gamma\psi) \qquad (53)$$

where $F(\gamma\psi)$ is the bending magnet formula from Eq. 21. This form clearly indicates the strong weakening of insertion device power as θ increases, vanishing at $\theta = \pm K/\gamma$.

Since $f_K(0,0)$ is normalized to unity, the radiated power density in the forward direction (i.e. along the undulator axis) is

$$\frac{d^2P}{d\theta d\psi}(\theta = 0,\psi = 0) = P_{total}\frac{21\gamma^2}{16\pi K}G(K) \qquad (54)$$

or, in practical units

$$\frac{d^2P}{d\theta d\psi}(\theta = 0,\psi = 0)[W/mrad^2] = 10.84B_0[T]E^4[GeV^4]I[A]NG(K) \qquad (55)$$

The total radiated power and forward power density values for selected undulators at NSLS, ALS, and APS are shown in Table 1. As is clearly evident from this table, the forward power density from undulators can be quite high, owing to their extremely narrow angular spread, while their total radiated power is relatively small.

Polarization of undulators and wigglers.

The polarization properties of the light emitted by wigglers, is similar to that of dipoles. For both sources the radiation is elliptically polarized when observed at some angle away from the orbital plane as given by Eq. 6. For radiation from planar undulators, however, the polarization is always linear. The polarization direction, which is in the horizontal plane when observed from that plane, rotates in a complicated way at other directions of observation. A comprehensive analysis of the polarization from undulators has been carried out by Kitamura[21]. The linear polarization of the undulator radiation is due to the symmetry of the

electron trajectory within each period. The polarization can in fact be controlled by a deliberate breaking of this symmetry. Circularly polarized radiation can be produced by a helical undulator, in which the series of dipole magnets is arranged each rotated by a fixed angle with respect to the previous one. For a variable polarization capability, one can use a pair of planar undulators oriented at right angles to each other. The amplitude of the radiation from these so-called crossed undulators is a linear superposition of two parts, one linearly polarized along the x direction and another linearly polarized along the y direction, x and y being orthogonal to the electron beam direction. By varying the relative phase of the two amplitudes by means of a variable-field magnet between the undulators, it is possible to modulate the polarization in an arbitrary way. The polarization can be linear and switched between two mutually perpendicular directions, or it can be switched between left and right circularly polarized. For this device to work, it is necessary to use a monochromator with a sufficiently small band-pass, so that the wave trains from the two undulators are stretched and overlap. Also the angular divergence of the electron beam should be sufficiently small or the fluctuation in relative phase will limit the achievable degree of polarization. A planar undulator whose pole boundaries are tilted away from a right angle with respect to the axial direction can be used as a helical undulator if the electron trajectory lies a certain distance above or below the mid-plane of the device.

Transverse Spatial Coherence.

As shown by Kim[22] and utilized in the brightness formulae given above, in wave optics the phase-space area of a radiation beam is given by the ratio of flux (F_0) to brightness (B_0). A diffraction limited photon beam (no electron size or angular divergence contribution) occupies the minimum possible phase-space area. From Eqs. 41-45 this area is:

$$\left(2\pi\sigma_r\sigma_{r'}\right)^2 = (2\pi\varepsilon)^2 = \left(\frac{\lambda}{2}\right)^2 \qquad (56)$$

Thus, the phase space occupied by a single Gaussian mode radiation beam is $(\lambda/2)^2$, and such a beam is referred to as completely transversely coherent. It then follows that the transversely coherent flux of a radiation beam is:

$$F_{coherent} = \left(\frac{\lambda}{2}\right)^2 B_o \qquad (58)$$

and the degree of transverse spatial coherence is

$$\frac{F_{coherent}}{F_0} = \left(\frac{\lambda}{2}\right)^2 \frac{B_o}{F_0}. \qquad (59)$$

Conversely, the number of Gaussian modes occupied by a beam is

$$\frac{F_0}{F_{coherent}} = \frac{F_0}{B_o(\lambda/2)^2}. \qquad (60)$$

Transverse spatial coherence is the quantity which determines the throughput of phase sensitive devices such as Fresnel zone plates used for x-ray microscopy. The degree of transverse spatial coherence of the various sources representative of synchrotron radiation shown in Fig. 11 is plotted in Fig. 13. It is clear from this figure that undulators on the lowest emittance storage rings provide the highest degree of transverse coherence, and are therefore the source of choice for x-ray microscopy.

In this chapter, we have attempted to compile the formulae needed to calculate the flux, brightness, polarization (linear and circular) and power produced by the three standard storage ring synchrotron radiation sources: bending magnets, wigglers and undulators. Where necessary, these formulae have contained reference to the emittance (ε) of the electron beam, as well as to the electron beam size (σ) and its divergence (σ'). For all three types of sources, the source phase space area, i.e. the spatial and angular extent of the effective (real) source, is a convolution of its electron and photon components. Modification of this effective beam size and divergence by drift along the direction of propagation and via interaction with optical elements (slits, pinholes, mirrors, gratings, crystals, zone plates, etc.) is most conveniently displayed by means of phase space diagrams. We will discuss the storage ring machine parameters which determine the source phase space area at any point around the ring, and leave the treatment of the other components, i.e. the beamlines, to the next section of this chapter.

The electron beam in a storage ring at a given point z around the ring may be described in the vertical (y-y') plane by the phase ellipse (see Fig. 14).

$$\gamma y^2 + 2\alpha y y' + \beta y'^2 = \textit{beam emittance}, \varepsilon, \qquad (59)$$

where $\alpha = -\beta/2 = -d\beta/2dz$ [23] and $\gamma = (\alpha^2+1)/\beta$ [22]. α, β, and γ are Twiss parameters[24] characterizing the beam.

As discussed earlier, electrons in circular orbits emit radiation with an energy spread depending on their energy and the radius of their orbit. There is also a characteristic vertical angular spread given by Eq. 12 which defines an rms divergence, σ_ψ that depends on the photon energy and is smaller for higher photon energies. For a particular wavelength, and using a one-σ_ψ contour, a photon phase ellipse such as that shown in Fig. 15 may be constructed from the electron phase ellipse depicted in Fig 14, through a convolution of the angular distributions of the electrons in the beam pipe and the photons emitted by each electron[23]. The equation for this new ellipse is

$$\left(\gamma + \frac{\sigma^2}{\varepsilon}\right) y^2 + 2\alpha y y' + \beta y'^2 = \varepsilon + \beta\sigma^2 \qquad (60)$$

Notice that the electron and photon ellipses have common spatial widths $2(\beta E)^{1/2}$, and common diameters, but that the photon beam has a larger angular divergence than the electron beam. This is the result of the addition in quadrature of the synchrotron radiation natural opening angle σ_ψ; the common diameter indicates that each electron emits photons symmetrically in angle with respect to the direction of its motion[25].

A photon beam that has propagated a distance z from the storage ring can be described by a photon phase ellipse with area $S_{sy} = \pi(\varepsilon[\varepsilon + \beta\sigma^2])^{1/2}$, maximum angular divergence $\Delta y'_m = 2(\varepsilon\gamma + \sigma^2)^{1/2}$, maximum spatial width $\Delta y_m = 2([\varepsilon\gamma + \sigma^2]z^2 - 2\alpha\varepsilon z + \beta\varepsilon)^{1/2} = 2([y'_m z]^2 - 2\alpha\varepsilon z + \beta\varepsilon)^{1/2}$, and constant source size (as seen by an observer looking along the z-axis) $\Delta y_o = 2S_{sy}/\pi\ y'_m$. These photon ellipses are described for one particular wavelength. Ellipses will differ for different wavelengths, due to a variation in the natural opening angle σ_ψ. Proper treatment of the electron beam phase space involves integrating the convolved electron beam/photon beam sizes/angular divergences over the source depth accepted by the beamline. See Green[23] and West and Padmore[26] for rather complete descriptions of this integration.

Fourth Generation Sources.

For completion we discuss fourth generation sources at least conceptually. These sources are of even higher brightness than the devices discussed in the preceeding text and are based on multi-particle coherence which can be understood as follows. In Fig. 1 the electric field induced by one electron, and hence the intensity, is proportional to the charge on an electron. If N electrons are circulating together in a storage ring, the emission is simply proportional to N times the emission of a single electron. However, when the electrons circulating in the storage ring, or passing through an insertion device, are close together compared to the wavelength of the light being emitted, the electric fields add coherently, so that the intensity scales like N^2. The electrons can be forced to micro-bunch when they are in the presence of the electric field of a superimposed light beam, and a magnetic field. The degree of multiparticle enhancement depends on the degree to which the microbunching occurs. In these devices a light beam either from a seed laser, or from back reflection of light spontaneously emitted from the same electrons in a previous pass through the device, causes the electrons to microbunch. New, even brighter sources of VUV radiation are being planned based on these principles.

References

1. A. Liénard, L'Eclairage Electrique **16**, 5 (1898).
2. J.P. Blewett, Nuclear Instr. & Methods **A266**, 1 (1988).
3. P.C. Hartman, Nuclear Instr. & Methods **195**, 1 (1982).
4. D.H. Tomboulian and P.L. Hartman, Phys. Rev. **102**, 1423 (1956).
5. J. Schwinger, Phys. Rev. **75**, 1912 (1949).
6. J.D. Jackson, "Classical Electrodynamics" (Wiley, New York) 1975.
7. H. Winick, "Synchrotron Radiation Research" (Plenum Press) Chapter 2 (1980).
8. A. Hofmann, Physics Reports **64**, 253 (1980).
9. S. Krinsky, M.L. Perlman and R.E. Watson, "Handbook of Synchrotron Radiation" ed. by E.E. Koch (North-Holland) Chapter 2 (1983).
10. K.J. Kim, "Physics of Particle Accelerators" AIP Proceedings **184**, 565 (1989).
11. A.A. Sokolov and I.M. Ternov, "Synchrotron Radiation" (Cambridge University Press) 1968.
12. V. O. Kostroun, Nuclear Instruments and Methods **172**, 371 (1980).
13. C.T.Chen, Review of Scientific Instruments **63**, 1229 (1992).
14. Born & Wolf, "Principles of Optics", Pergamon Press (1964).
15. Lawrence Berkeley Laboratory Publication 643 Rev. 2 (1989).
16. S. L. Hulbert and J. M. Weber, Nucl. Instruments and Methods **A319**, 25 (1992).
17. R.P. Walker and B. Diviacco, Rev. of Scientific Instruments **63**, 392 (1992).
18. R.P. Dejus and A. Luccio, Nucl. Instruments and Methods **A347**, 61 (1994).
19. M.R. Howells and B.M. Kincaid, LBL Report #34751 (1993).
20. K.J. Kim, Nuclear Instruments and Methods **A246**, 67 (1986).
21. H. Kitamura, Japanese Journal of Applied Physics **19** L185 (1980).
22. K.J. Kim, Nuclear Instruments and Methods **A246**, 71 (1986). See also earlier work of A.M. Kondratenko and A.N. Skrinsky, Opt. Spectroscopy **42** 189 (1977) and F. Zernike, Physica V, 785 (1938).
23 G. K. Green, BNL Rept. 50522 (1976), G. K. Green, BNL Rept. 50595 (1977).
24. E.D. Courant and H.S. Snyder, Annals of Physics **3**, 1 (1958).
25. T. Matsushita and U. Kaminaga, J. Appl. Cryst. **13**, 464 (1980).
26. J.B. West and H.A. Padmore, Optical Engineering, in Handbook on Synchrotron Radiation, vol. 2, ed. G.V.Marr, p. 21 (1987).

ID	E(GeV)	B_o(T)	I(A)	λ_u(cm)	N	K	P_{total}(W)	$\frac{d^2P}{d\theta d\psi}(\theta = 0, \psi = 0)$ [W/mrad^2]
NSLS U5	0.8	0.25	0.8	7.5	27	1.75	41	23.4
ALS U8.0	1.9	0.23	0.4	8.0	27	1.75	104	343
ALS U5.0	1.9	0.37	0.4	5.0	44	1.75	275	898
NSLS X1	2.584	0.23	0.5	8.0	35	1.75	313	1900
APS UA	7.0	0.57	0.2	3.3	36	1.75	2394	104315

Table 1

Figure Captions

Fig. 1. Conceptual representation of the radiation pattern from a charged particle undergoing circular acceleration at (a) sub-relativistic and (b) relativistic velocities.

Fig. 2. Illustration of the derivation of the spectrum emitted by a charged particle in a storage ring.

Fig. 3. Universal synchrotron radiation output curve.

Fig. 4. Plot of the function C(y) defined in Eq. 13.

Fig. 5. Normalized intensities of horizontal and vertical polarization components, as functions of the vertical observation angle for different photon energies.

Fig. 6. P_c vs. $\gamma\psi$ vs ω/ω_c for E=0.8 GeV, ρ=1.91m.

Fig. 7. Vertical angle dependence of bending magnet power, $F(\gamma\psi)$ vs. $\gamma\psi$.

Fig. 8. Schematic of an insertion device.

Fig. 9. Conceptual representation of the electric fields emitted as a function of time by an electron in (a) a wiggler, and (b) an undulator, with the corresponding spectra.

Fig. 10. Spectral output and angular distribution of the emission from the NSLS In-Vacuum UNdulator (IVUN) for K=0.75. (a) spectral output in the forward direction, with (solid line) and without (dotted line) the effect of electron beam emittance; (b) angle-integrated spectral output with (solid line) and without (faint solid line) the effect of electron beam emittance, and the decomposition into harmonics (n=1,2,3,4) (dotted lines); (c) angular distribution of the first three harmonics (n=1,2,3), with and without the effect of electron beam emittance. The emittance of the NSLS X-ray ring is 94nm horizontal and 0.1nm vertical.

Fig. 11. Output flux for various synchrotron sources.

Fig. 12. Output brightness for various synchrotron sources.

Fig. 13. Degree of transverse spatial coherence.

Fig. 14. Storage ring electron beam phase space ellipse.

Fig. 15. Photon phase space ellipse.

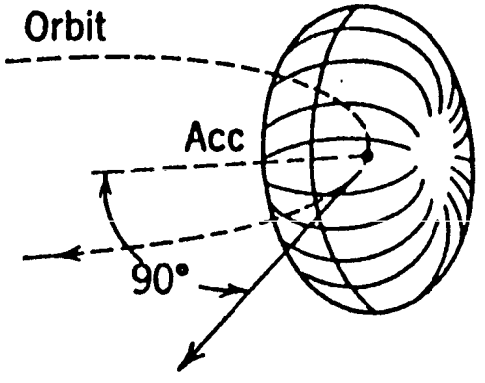

(a)

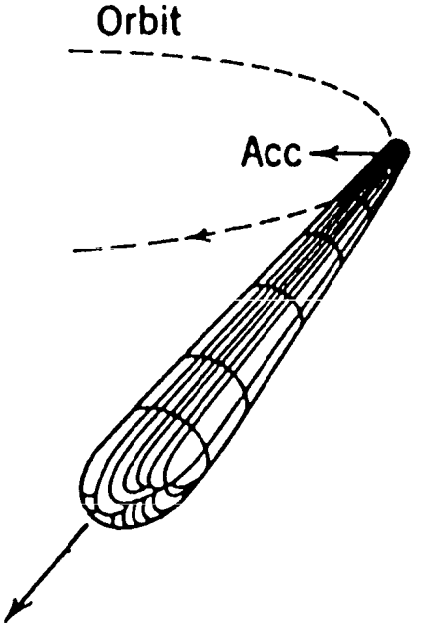

(b)

Hulbert/Williams

$$\Delta t' = \frac{\rho}{c\gamma}$$

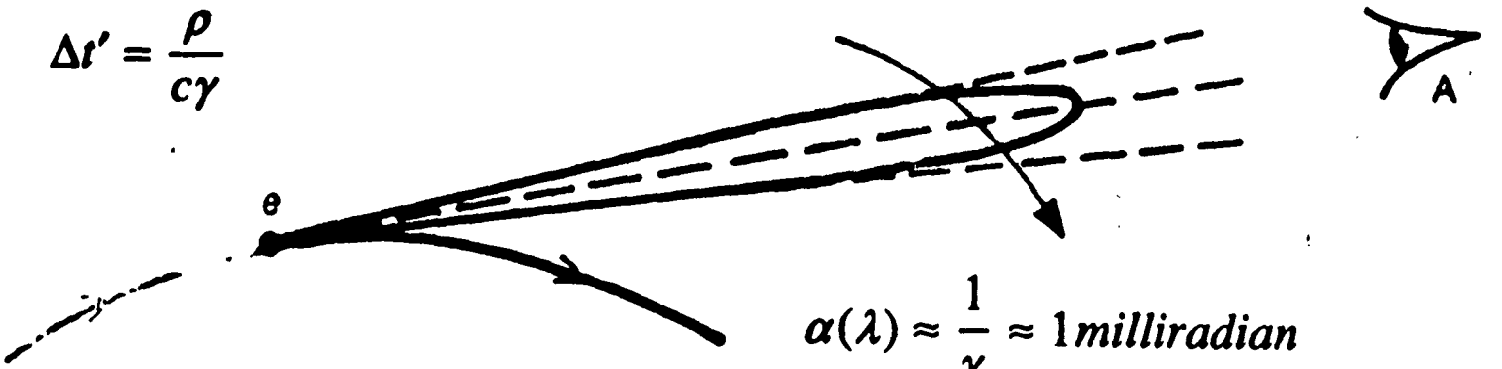

$$\alpha(\lambda) \approx \frac{1}{\gamma} \approx 1 milliradian$$

$$\Delta t = \frac{1}{\gamma^2} \times \frac{\rho}{c\gamma} = \frac{2}{10^9 \times 3 \times 10^8}$$

b

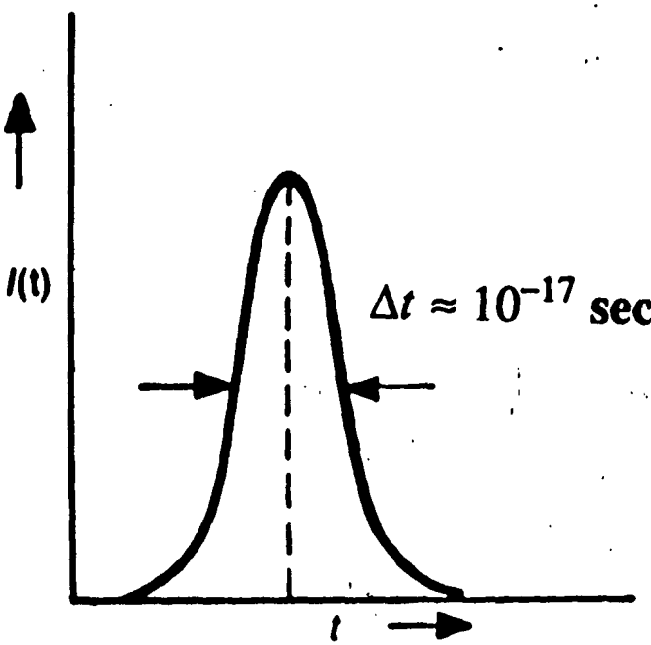

$\Delta t \approx 10^{-17}$ secs.

c

$$\omega_c \approx \frac{1}{\Delta t} \approx 30 Angstroms$$

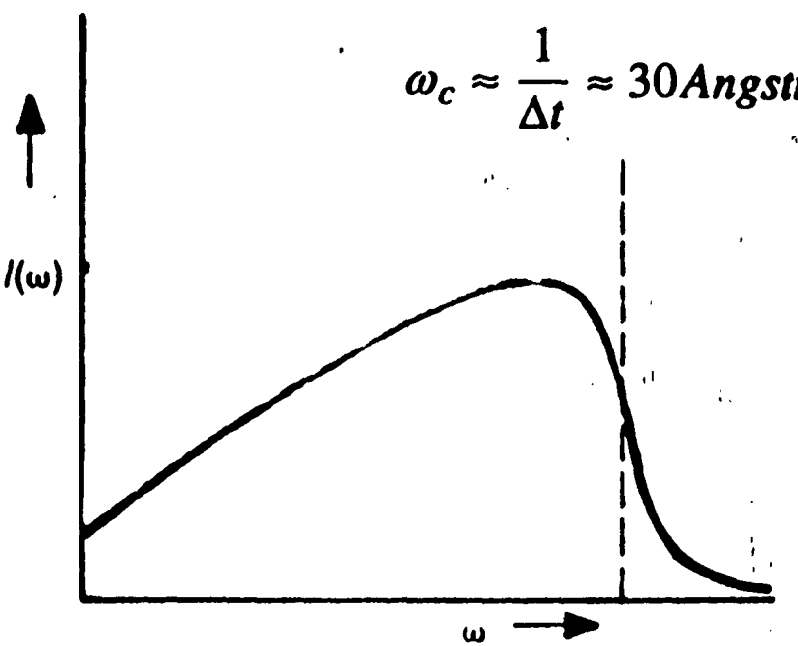

Hulbert/Williams

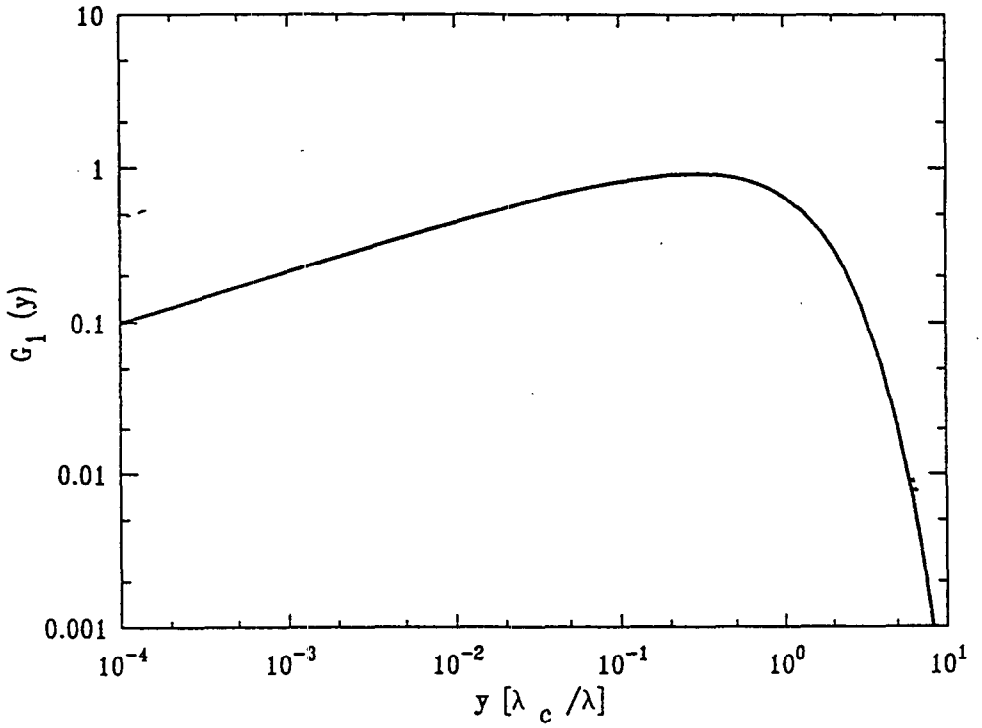

Hulbert/with c

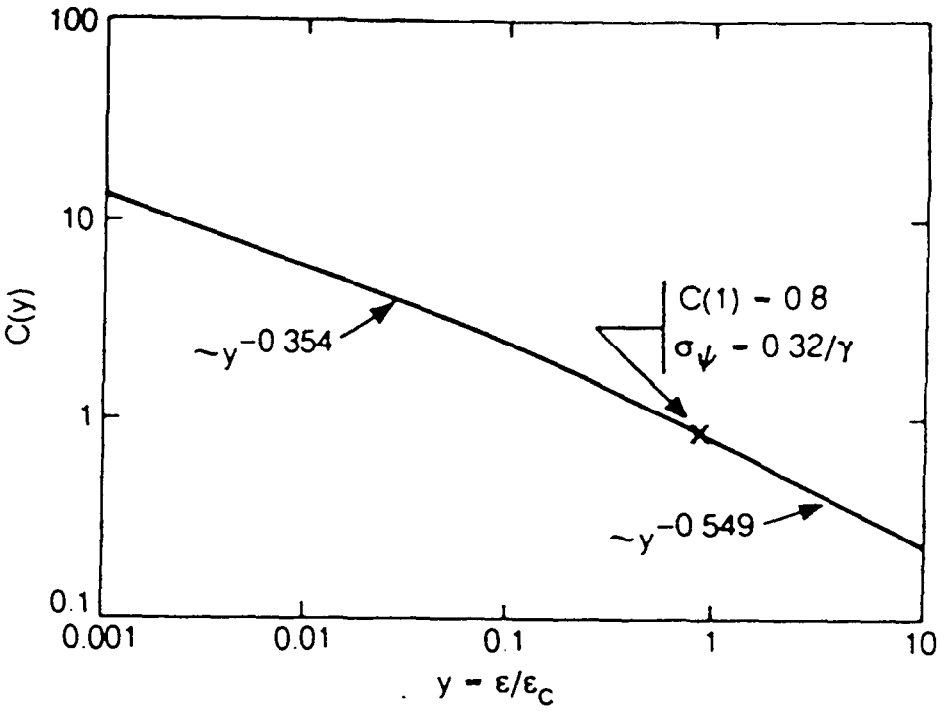

Hubert Williams

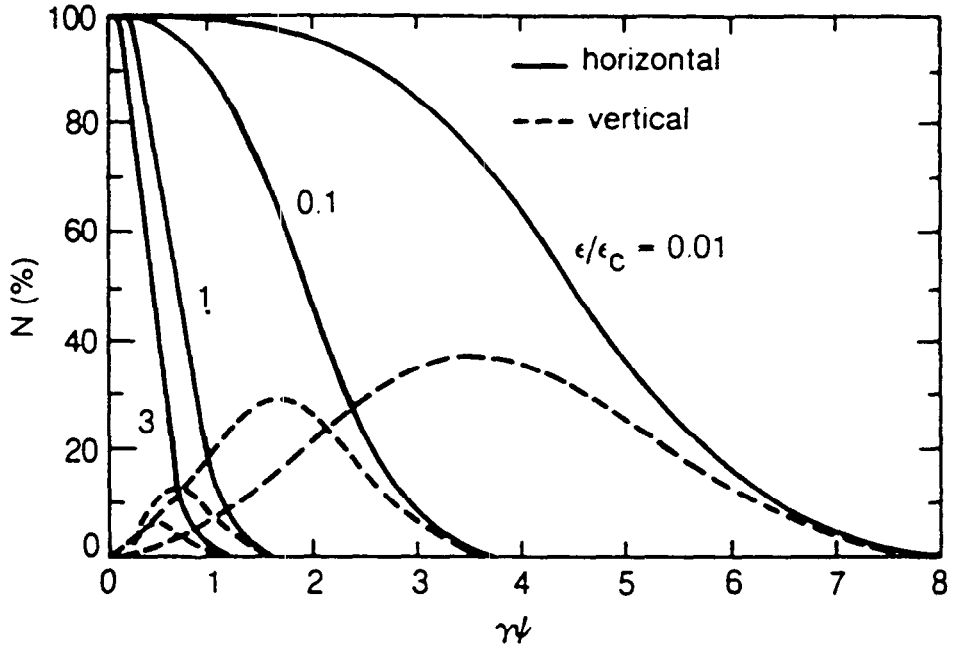

Hulbert/vertical

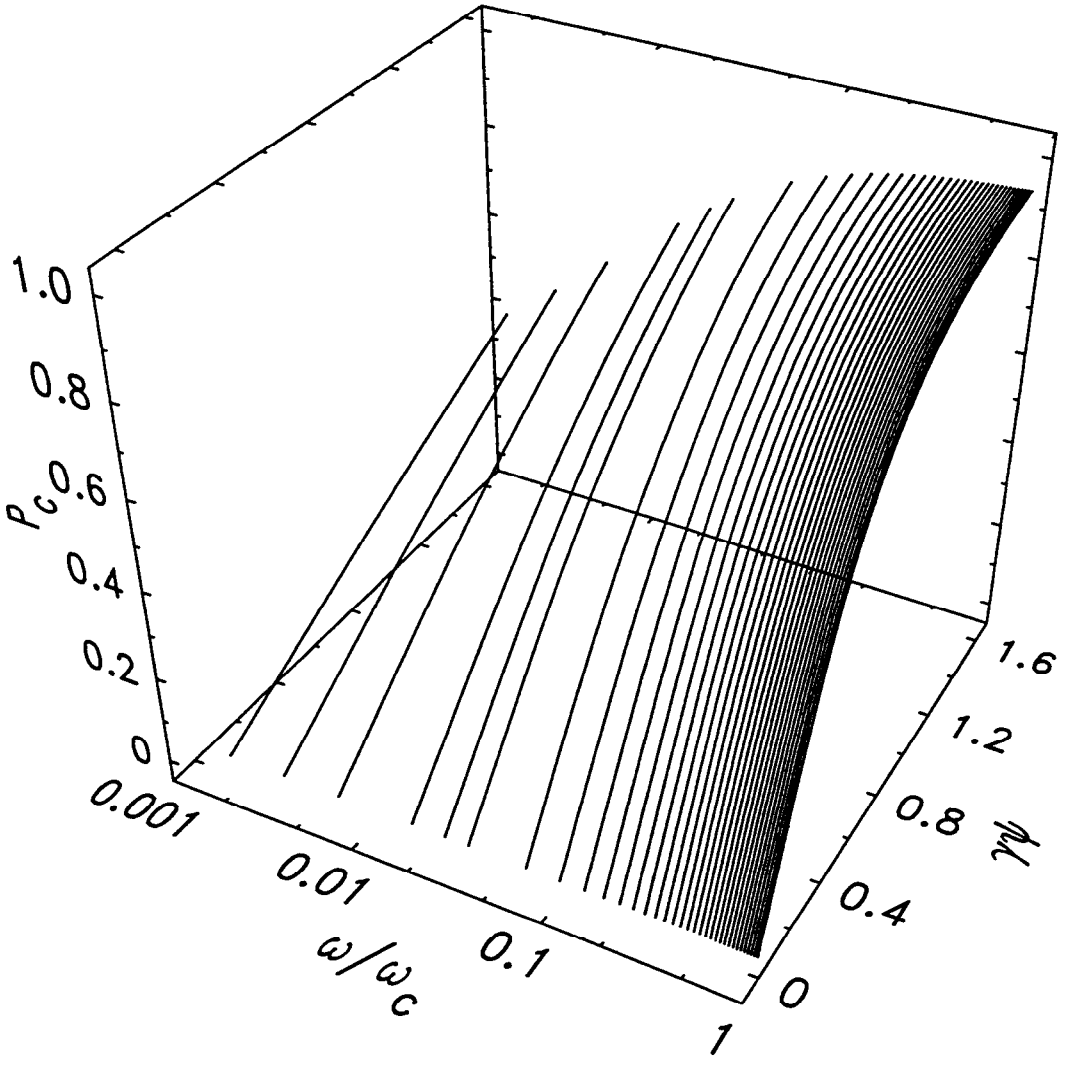

Hulbert, Williams
Fig 5

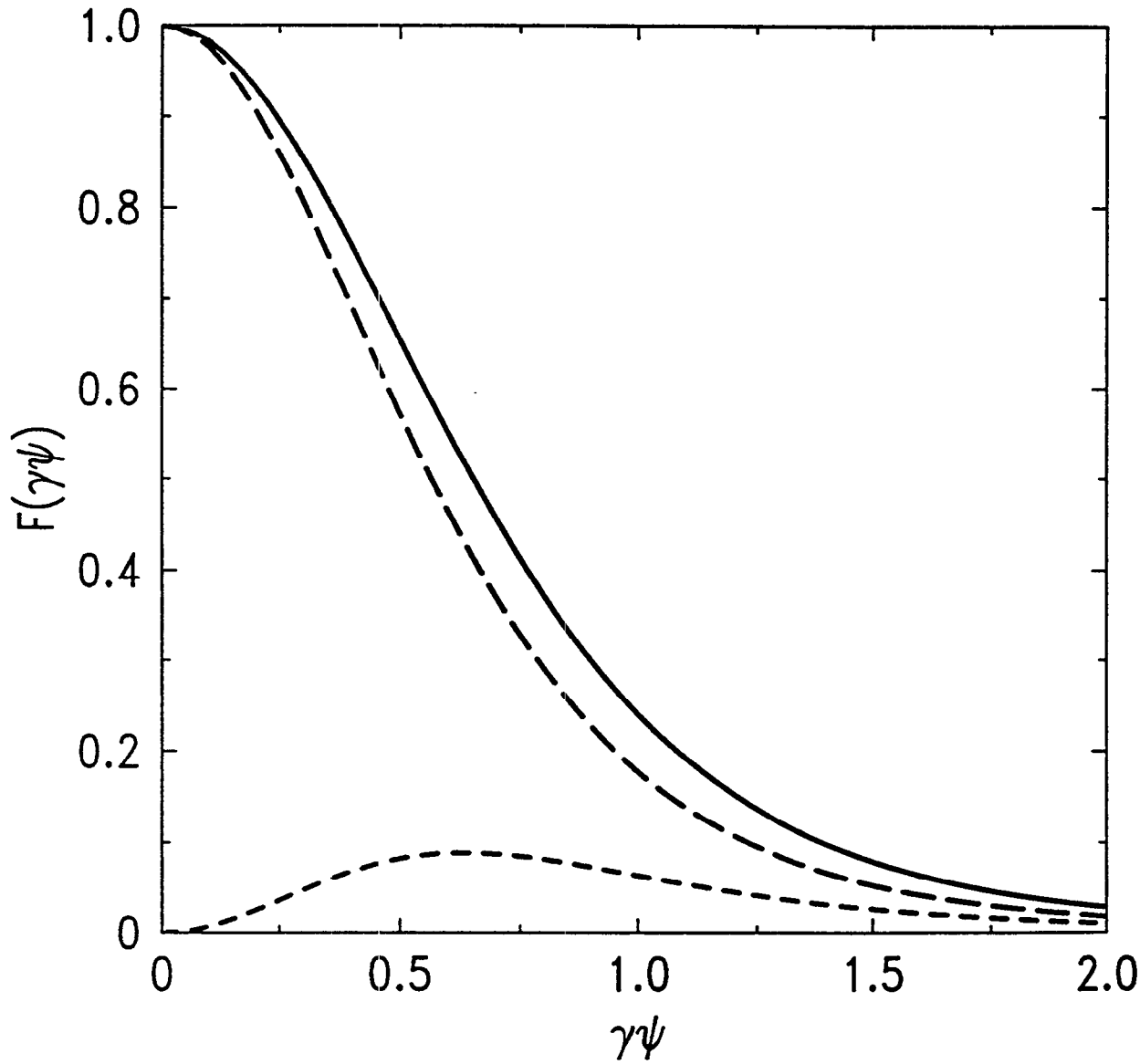

Hulbert/Hoffman

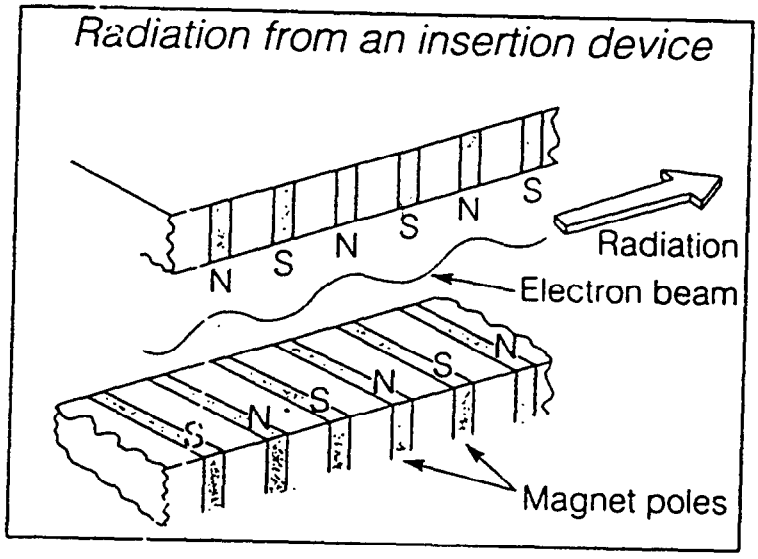

Hulbert/Williams

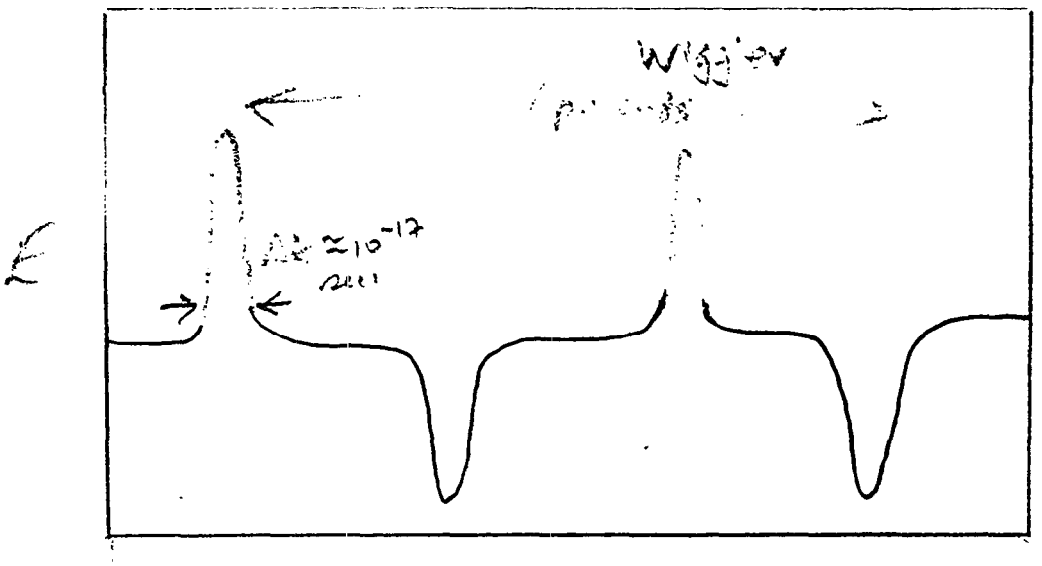

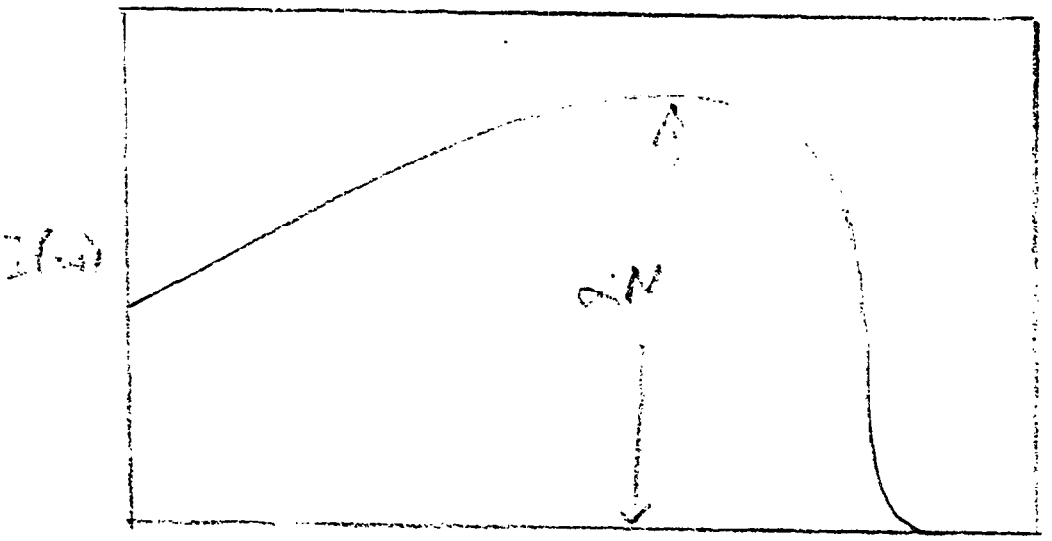

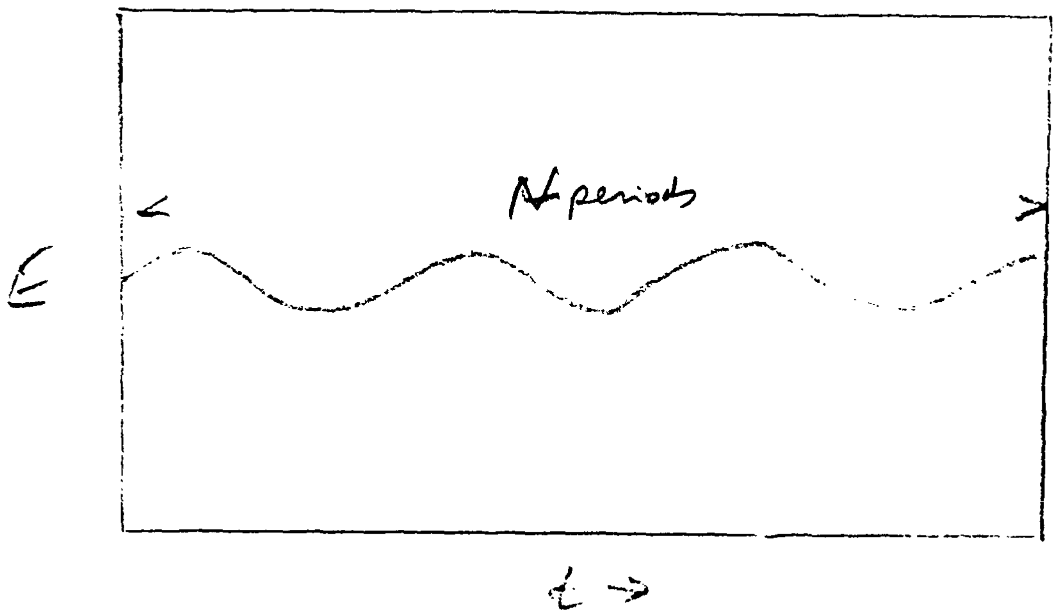
N periods
E
t →

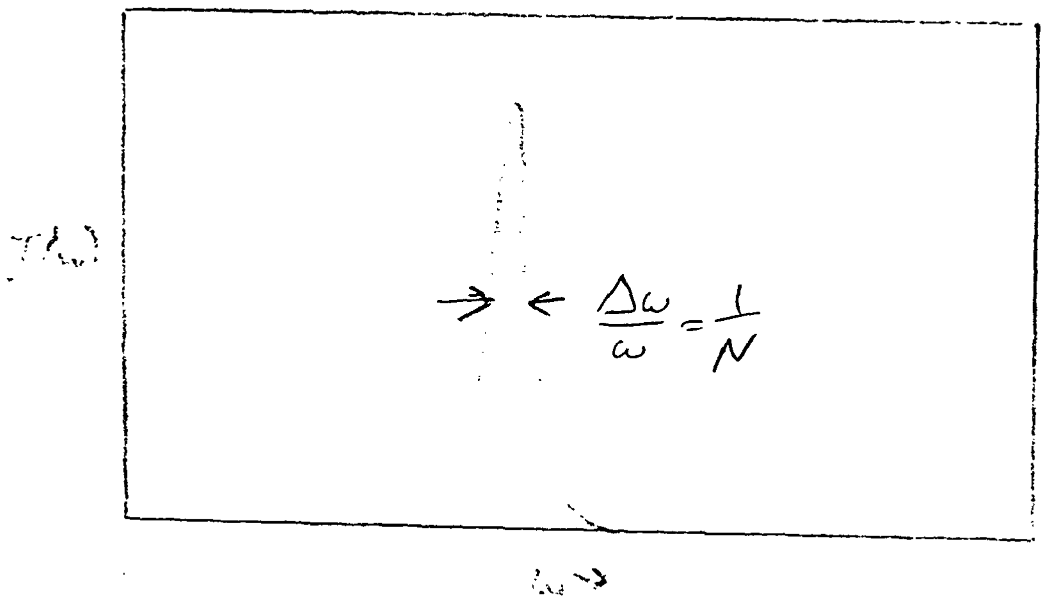
→ ← Δω/ω = 1/N

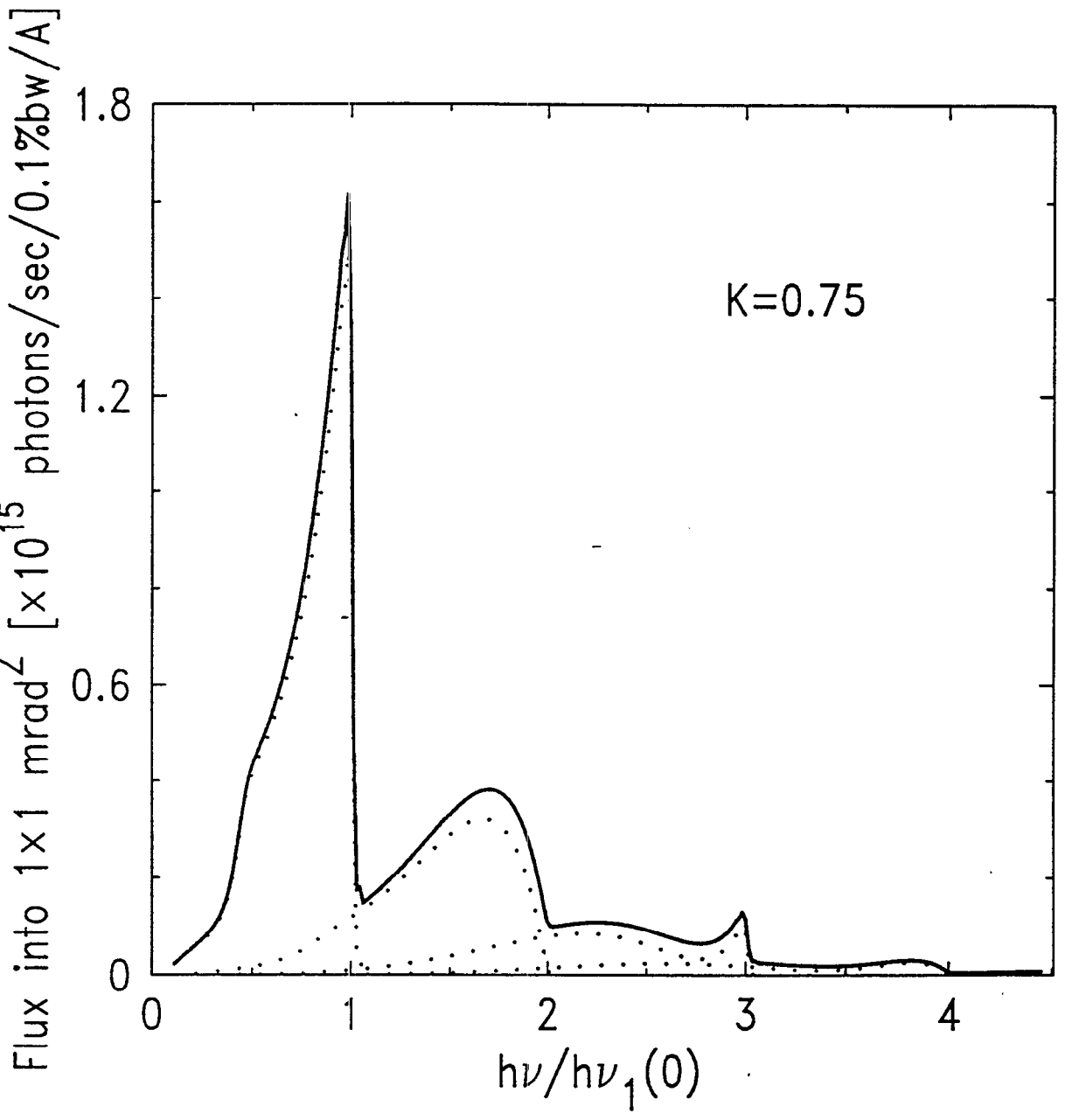
Flux into 1×1 mrad^2 [×10^{15} photons/sec/0.1%bw/A]
1.8
1.2
0.6
0
0
1
2
3
4
hν/hν$_1$(0)
K=0.75

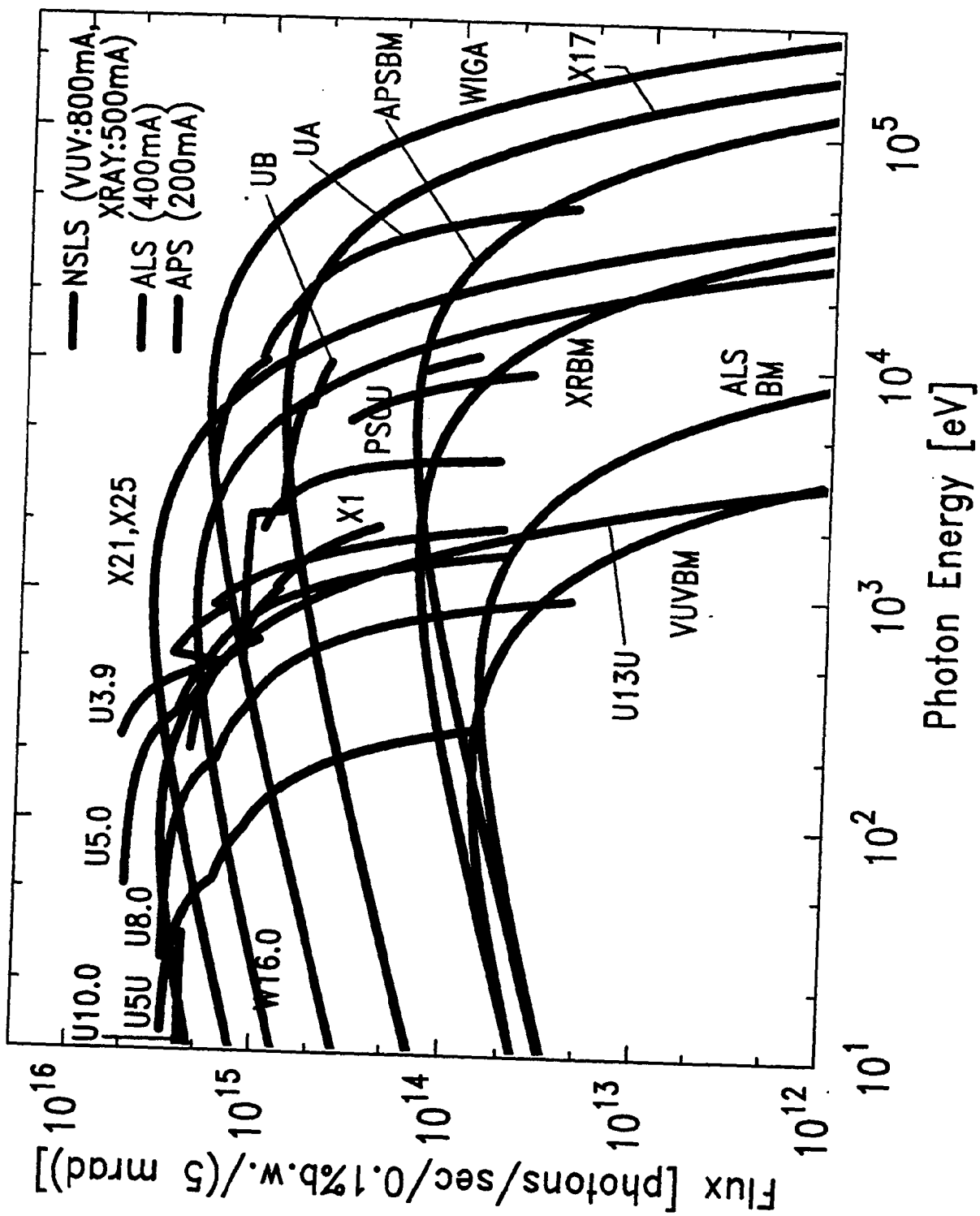
NSLS (VUV:800mA, XRAY:500mA)
ALS (400mA)
APS (200mA)
U10.0
U5U
U8.0
U5.0
U3.9
X21,X25
WT6.0
X1
PSU
UB
UA
APSBM
WIGA
X17
XRBM
ALS BM
U13U
VUVBM
Flux [photons/sec/0.1%b.w./(5 mrad)]
Photon Energy [eV]

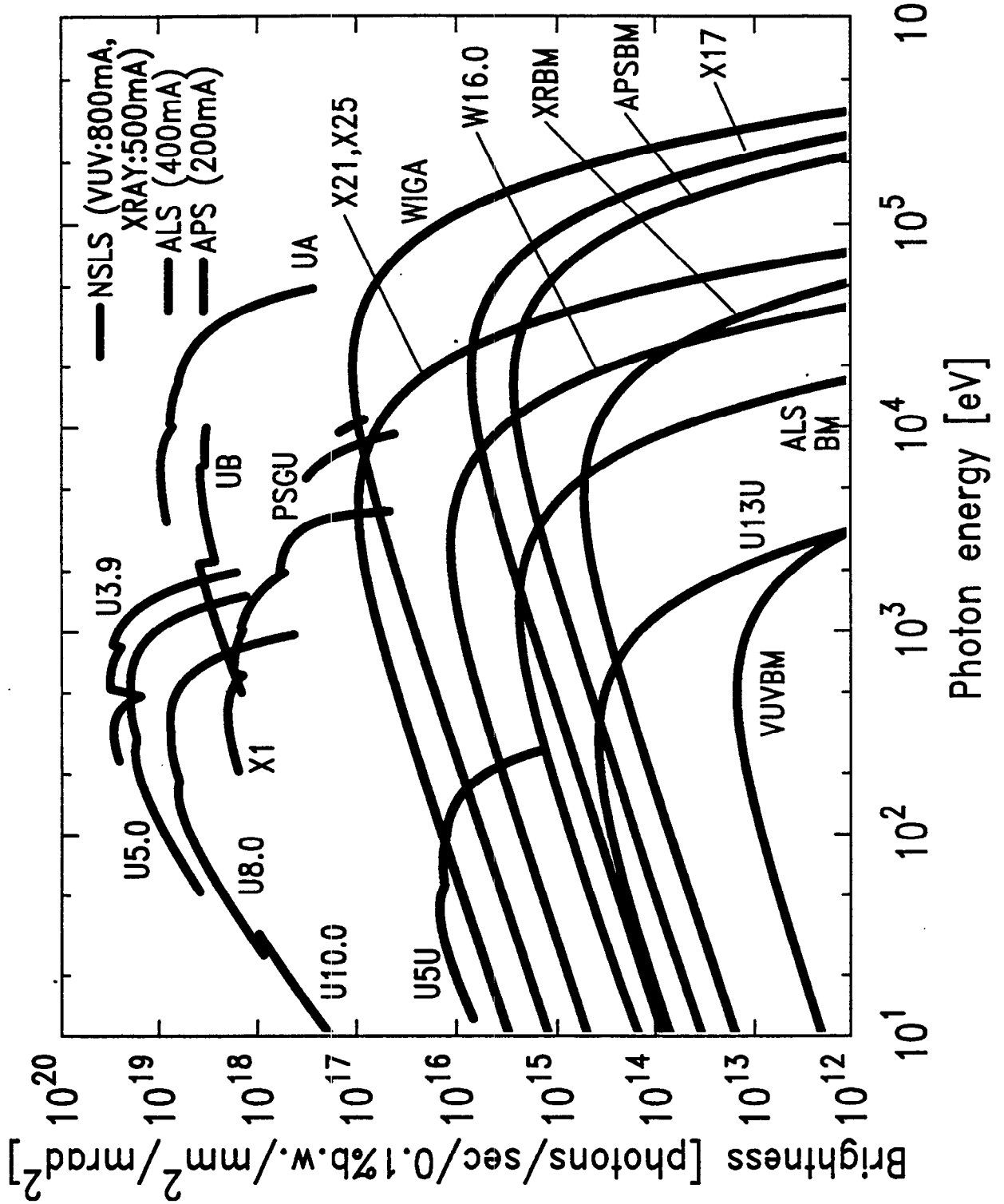

Hulbert written on 12

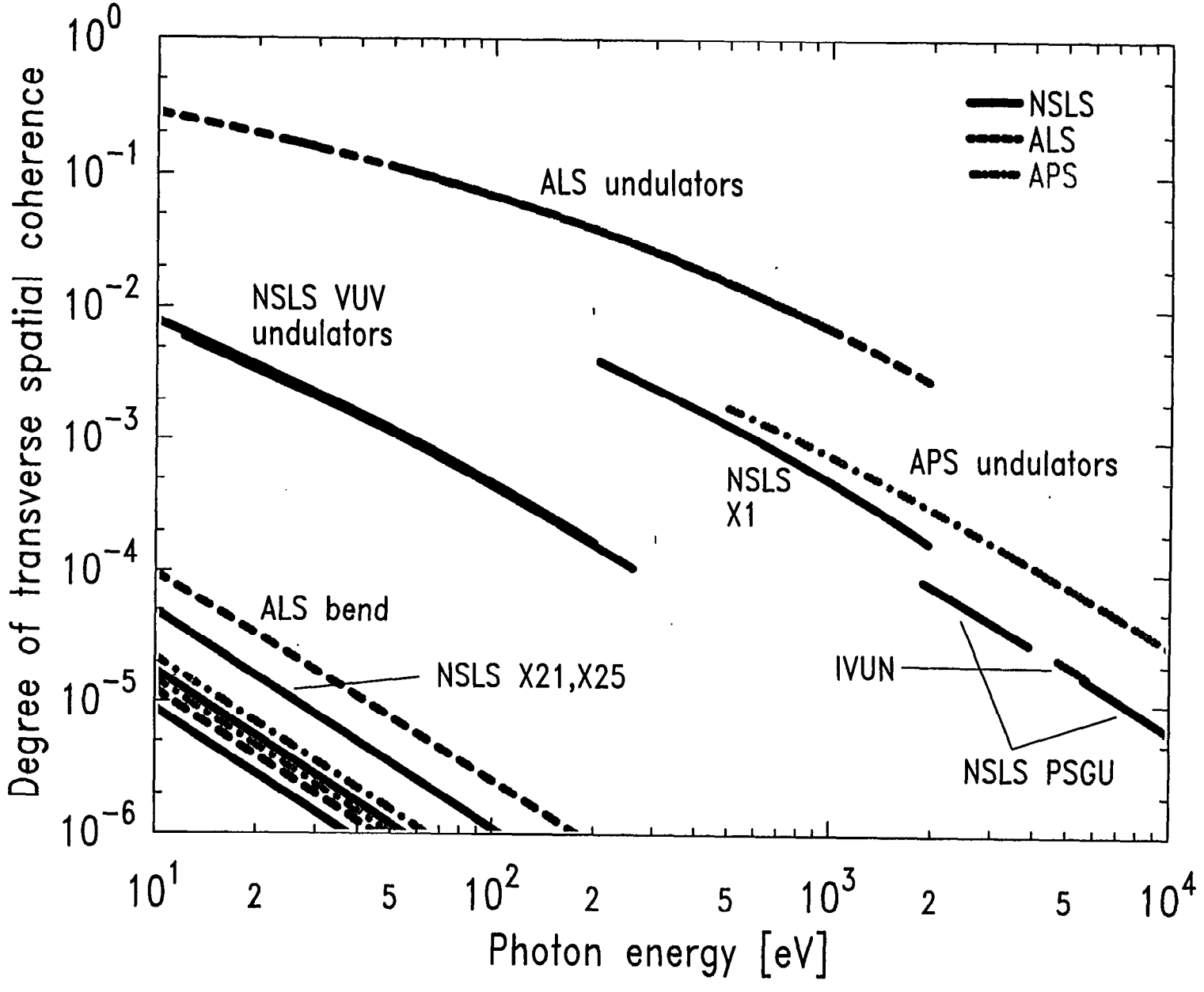

Hulbert/Williams
FG13

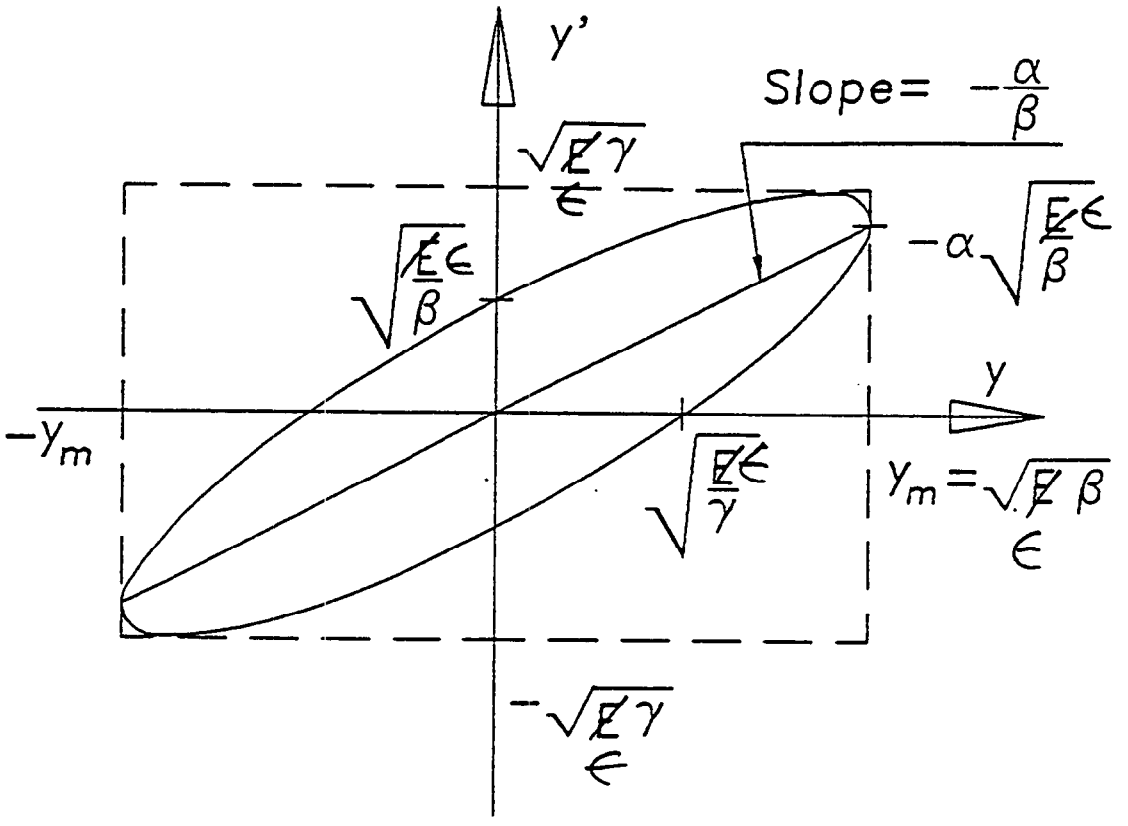

Storage ring electron beam phase ellipse.

Hulbert/Wiltsam

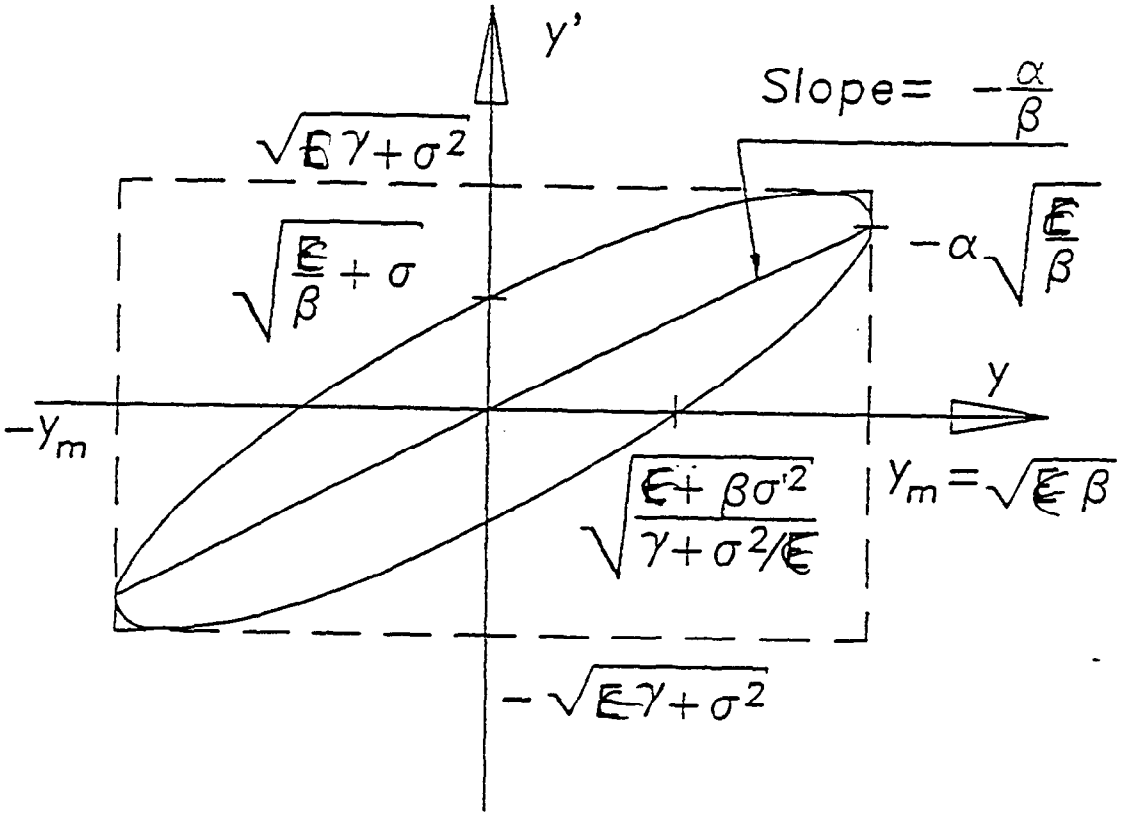

Hulbert/William
F6 15